

# THz Electrodynamics of Mixed-Valent YbAl<sub>3</sub> and LuAl<sub>3</sub> Thin Films

D. Barbalas,<sup>1</sup> S. Chatterjee,<sup>2,3</sup> D.G. Schlom,<sup>4,5,6</sup> K. M. Shen,<sup>2,5</sup> and N. P. Armitage<sup>1</sup>

<sup>1</sup>*Department of Physics and Astronomy, The Johns Hopkins University, Baltimore, MD 21218, USA*

<sup>2</sup>*Laboratory of Atomic and Solid State Physics, Department of Physics,  
Cornell University, Ithaca, New York 14853, USA*

<sup>3</sup>*Department of Electrical & Computer Engineering,  
University of California, Santa Barbara, CA 93106, USA*

<sup>4</sup>*Department of Materials Science and Engineering,  
Cornell University, Ithaca, New York 14853, USA*

<sup>5</sup>*Kavli Institute at Cornell for Nanoscale Science, Ithaca, New York 14853, USA*

<sup>6</sup>*Leibniz-Institut für Kristallzüchtung, Max-Born-Str. 2, 12489 Berlin, Germany*

(Dated: April 13, 2022)

We present THz measurements of thin films of mixed-valent YbAl<sub>3</sub> and its structural analogue LuAl<sub>3</sub>. Combined with traditional Fourier transform infrared (FTIR) spectroscopy, the extended Drude formalism is utilized to study the low-frequency transport of these materials. We find that LuAl<sub>3</sub> demonstrates conventional Drude transport whereas at low temperatures YbAl<sub>3</sub> demonstrates a sharply renormalized Drude peak and a mid-infrared (MIR) peak in the conductivity, indicative of the formation of a heavy Fermi liquid. In YbAl<sub>3</sub> the extended Drude framework shows a consistency of the scattering rate with Fermi-liquid behavior below  $T < 40$  K and a moderate mass enhancement. While a  $\omega^2$  Fermi liquid-like frequency dependence is not clearly exhibited, the temperature dependence of the Drude scattering rate and effective mass is consistent with the formation of a low-temperature moderately heavy Fermi liquid, albeit one with a smaller mass than observed in single crystals. The extended Drude analysis also supports a slow crossover between the Fermi liquid state and the normal state in YbAl<sub>3</sub>.

## INTRODUCTION

Rare-earth intermetallic systems demonstrate a wide variety of low-temperature behavior due to the interplay between electronic correlations and local moment physics. At low temperatures, Kondo physics dominates and the screening of the  $f$ -electrons leads to the formation of a Fermi-liquid (FL) of heavy quasi-particles below a temperature  $T^*$ , giving their name to the heavy fermion (HF) class of materials. These HF materials demonstrate a wide variety of exotic physics including non-conventional superconductivity and quantum phase transitions [1, 2]. Related to the class of HF compounds are the family of mixed-valence (MV) materials which demonstrate weaker localization of the  $f$ -orbitals, allowing the interplay of both charge and spin degrees of freedom [3]. These materials are characterized by a significantly larger Kondo scale with respect to the Fermi liquid scale, i.e.  $T_K \gg T^*$ . While the mixed-valence case is expected to smoothly evolve out of the HF state, there remains many unique phenomena that can arise. Due to their well-separated energy scales, these systems can be tuned to study a variety of emergent phenomena in strongly correlated materials.

The core physics of mixed valence materials can be described using the Anderson lattice model [2, 4–6]. While  $f$ -orbital systems generically exhibit qualitative behaviors consistent with the Anderson impurity model formulation, the generalization of the single impurity to the lattice model has remained difficult to treat [7]. Based on the nature of the screening processes occurring, exten-

sions to the lattice models can give predictions for how the crossover between the low-temperature Fermi liquid behavior and the normal state should occur. The concept of a slow crossover arises due to extended screening processes that exist in the lattice model that are not explicitly described in the single impurity model. Despite extensive studies of lanthanide intermetallic compounds, uncertainty still exists as to why Yb-based correlated materials do not show the same broad range of correlated phenomena as compared to other lanthanide series elements; most notably, there has historically been a stark absence of Yb-based materials that demonstrate unconventional superconductivity. Naïvely, the commonality between Ce ( $4f^1$ ) and Yb ( $4f^{13}$  in Yb<sup>+3</sup>) compounds as  $4f$  electron-hole counterparts would suggest that they would share a similar range of behaviors; however, experimentally this has not been found to be the case [8, 9]. For instance, no Yb-based system had demonstrated unconventional superconductivity until the discovery in  $\beta$ -YbAlB<sub>4</sub> with  $T_c = 80$  mK [10]. The presence of a non-FL state with superconductivity at low temperatures is evidence that the system inherently resides near a quantum critical point in the phase diagram without the need for tuning by external pressure. This recent discovery of a historically elusive phenomena in Yb-based materials highlights the opportunities that exist by revisiting previously studied materials.

In YbAl<sub>3</sub>, the Yb ion demonstrates a mixed valence state between Yb<sup>2+</sup> and Yb<sup>3+</sup> with a large separation of energy scales between the heavy Fermi liquid (FL) coherence temperature  $T^* = 34 - 40$ K and the Kondo

temperature  $T_K \approx 670$  K [11]. Consistent with heavy FL quasiparticles forming at low temperatures, there exists a sharply renormalized Drude peak due to the formation of heavy-quasiparticles and a mid-infrared peak corresponding to excitations between the hybridized conduction and  $f$ -electron bands [12, 13]. The existence of a moderately heavy FL state is supported by experimental results for the specific heat coefficient  $\gamma = 40$  mJ/mol K and the measured dHvA effective mass below 1.5K of  $m^* = 15 - 30m_e$  [11, 13–15]. Recent ARPES spectroscopy on YbAl<sub>3</sub> and LuAl<sub>3</sub> thin films has also uncovered that valence fluctuations drive a Lifshitz transition at 21K by shifting the chemical potential [16]. These recent results suggest that interplay of mixed-valence and Kondo physics can lead to previously unexpected low-temperature behaviors which deserve closer study.

In this work we present the optical response of thin films of YbAl<sub>3</sub> and their structural analogue LuAl<sub>3</sub> characterized by time-domain THz spectroscopy (TDTS) and Fourier-transform IR spectroscopy (FTIR). The low-energy scale accessible by our THz spectral range of 0.1-8 meV allows for the direct characterization of low-energy excitations of hybridized states as a function of both frequency and temperature. Using the extended Drude formalism, we observe that the quasiparticle scattering rate shows temperature scaling consistent with Fermi liquid theory in YbAl<sub>3</sub> whilst LuAl<sub>3</sub> demonstrates behavior consistent with a simple non-interacting metal. The effective mass demonstrates a gradual temperature-dependent crossover suggestive of non-negligible coupling of Yb  $f$ -electrons to the Al conduction band occurring at intermediate temperatures above  $T^* = 37$ K.

## EXPERIMENTAL DETAILS

The (001)-oriented thin films of YbAl<sub>3</sub> and LuAl<sub>3</sub> used in this study were 15 nm thick and grown on (001) MgO substrates using molecular-beam epitaxy (MBE). For all films, a 0.8 nm thick aluminum buffer layer was first deposited. This allowed the growth of continuous, smooth films of LuAl<sub>3</sub>/YbAl<sub>3</sub>. In these studies, we investigated a 20 nm thick LuAl<sub>3</sub> film and a 15 nm thick YbAl<sub>3</sub> film. The YbAl<sub>3</sub> was synthesized on top of a 5 nm thick LuAl<sub>3</sub> buffer layer on top of the Al buffer, which improved the quality of the YbAl<sub>3</sub> layer. All films were capped with 2 nm thick layer of Al. Characterization of these films was conducted using x-ray diffraction, low energy electron diffraction and scanning transmission electron spectroscopy. Despite the dramatic advances in growing such films by MBE, it is important to note that the residual resistivity ratio ( $\text{RRR} = \rho(300 \text{ K})/\rho(5 \text{ K})$ ) of the YbAl<sub>3</sub> film is still much less than the approximately 60 found in high quality single crystals [14]. More details about the thin film growth and characterization can be found elsewhere [17].

The low-energy response of the films were characterized using time-domain THz spectroscopy (TDTS). In TDTS, an approximately single-cycle ps long pulse of radiation is transmitted through the sample. One takes the Fourier transform of the transmitted electric field and references it to the signal through a bare MgO substrate to get the complex transmission of the thin films. An advantage of the technique is that the complex conductivity can be directly extracted from the complex transmission without a Kramers-Kronig transform. The complex conductivity  $\tilde{\sigma}$  can be determined from the transmission by,

$$\tilde{T}(\omega) = \frac{n_s + 1}{n_s + 1 + Z_0 d \tilde{\sigma}(\omega)} e^{i \frac{\omega}{c} \Delta L (n_s - 1)}, \quad (1)$$

where  $n_s$  is the substrate index of refraction,  $Z_0$  is the impedance of free space,  $d$  is the sample thickness,  $\tilde{\sigma}$  is the complex conductivity,  $\omega$  is the frequency,  $c$  is the speed of light, and  $\Delta L$  is a correction factor due to the difference in thickness between the substrate and the sample.

In order to isolate the conductance of the LuAl<sub>3</sub>/YbAl<sub>3</sub> samples from the buffer and capping layers, a reference film comprised of the buffer and capping layers (without a sample film) was used to correct for the presence of parallel conductance channels. By subtracting the conductance of the buffer layers from the total conductance of the sample films, the conductivity of the LuAl<sub>3</sub>/YbAl<sub>3</sub> layer could be obtained.

In tandem with the THz measurement, the mid-IR (MIR) response (400-7500 cm<sup>-1</sup>, 0.05 - 930 meV) was studied using conventional Fourier-transform infrared (FTIR) spectroscopy down to 5 K. Transmission experiments were measured using a commercial FTIR spectrometer (Bruker Vertex 80V) using a Globar source and a solid-state DTGS detector.

## RESULTS

In Fig. 1, the DC resistivity of films of the two materials are shown. At the lowest temperatures, the YbAl<sub>3</sub> film demonstrates a  $\rho \propto T^2$  dependence as shown previously [16]. The resistivity saturates above some temperature  $T^*$  that is of order 200 K. The resistivity of the LuAl<sub>3</sub> film shows a monotonic decrease with decreasing temperature.

In Fig. 2 we present the real and imaginary parts of the THz conductivity for YbAl<sub>3</sub> and LuAl<sub>3</sub> at different temperatures. At high temperatures, both films demonstrate large scattering rates indicated by the flat, nearly frequency independent real conductivity. Upon cooling the scattering rate decreases in both films; however, in YbAl<sub>3</sub>, the decrease is significantly larger. In the case of YbAl<sub>3</sub> sample, at the lowest temperatures there is an increase in the low-frequency spectral weight as seen by the enhancement of the real and imaginary parts of the

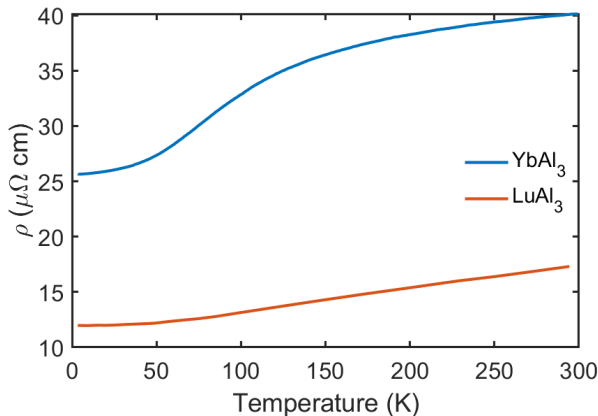


FIG. 1. DC resistivity as a function of temperature for the YbAl<sub>3</sub> and LuAl<sub>3</sub> thin films.

conductivity over the room temperature state. We believe this consistent with the formation of a narrow Drude peak at the lowest temperatures. This is in contrast to the LuAl<sub>3</sub> film, which is characterized by a broad Drude-like contribution to the conductivity without a major temperature dependence of the scattering rate.

The MIR transmission of the YbAl<sub>3</sub> and LuAl<sub>3</sub> thin films are shown in Fig. 3. Using both the THz complex conductivity and the MIR transmission, the optical conductivity was modeled using Drude-Lorentz parameterization in the fitting software reFFIT [18]. The LuAl<sub>3</sub> data was fit by two Drude terms, whereas the fit to the YbAl<sub>3</sub> data used two Drude terms and a single high frequency Drude-Lorentz oscillator. Due to strong absorption of the underlying MgO substrate, the FIR transmission below 1000 cm<sup>-1</sup> was not accessible. Hence, in the FIR region without experimental data, the modeled conductivity determined through the Kramers-Kronig consistent fitting can only give a rough guide, but is not a definitive measure of the conductivity.

From the MIR data on the YbAl<sub>3</sub> thin film, we see a clear MIR conductivity peak suggestive of a hybridization gap [19], which becomes enhanced as the temperature decreases. The position of the MIR conductivity peak in YbAl<sub>3</sub> is centered around  $\omega = 2800$  cm<sup>-1</sup>; the corresponding value in single crystals has been found to be centered at  $\omega \sim 2000$  cm<sup>-1</sup>. While there is no strain expected to arise from the underlying Al and LuAl<sub>3</sub> buffer layers on MgO, this shift in the conduction electron-4*f* hybridization resonance can be attributed to the effects of strong impurity scattering [20].

## DISCUSSION

From the comparison of the optical response of LuAl<sub>3</sub> to YbAl<sub>3</sub>, it appears that the full *f*-orbital in the Lu

compound prevents the development of the heavy quasiparticles as seen in the YbAl<sub>3</sub> film. In order to address the complex quasiparticle behavior, it is useful to use the framework of the extended Drude model by allowing the scattering rate and effective mass to take on both frequency and temperature dependence [21]. These quantities can be arrived at in a model-free fashion by inverting the complex conductivity as,

$$\frac{m^*(\omega)}{m_b} = -\frac{\omega_p^2}{4\pi\omega} \text{Im} \left[ \frac{1}{\sigma(\omega)} \right], \quad (2)$$

$$\frac{1}{\tau(\omega)} = \frac{\omega_p^2}{4\pi} \text{Re} \left[ \frac{1}{\sigma(\omega)} \right], \quad (3)$$

where  $m_b$  is the band mass and  $\omega_p$  is the intraband plasma frequency. The exact value of the plasma frequency only serves to scale the renormalized mass and scattering rate and has no impact on their temperature and frequency scaling.

The intraband plasma frequency was determined by adding the spectral weight of each of the fitted low-frequency Drude oscillators up to the intraband cutoff frequency  $\omega_c$ . The cutoff is often defined as where  $\sigma_2 \rightarrow 0$  or where  $\sigma_1$  demonstrates a minimum, as shown in Fig. 3. This allows the intraband plasma frequency to be extracted from the spectral weight by the *f*-sum rule, given as:

$$\int_0^{\omega_c} \sigma^{intra}(\omega) d\omega = \frac{\omega_p^2}{8}, \quad (4)$$

In order to determine the intraband plasma frequency, the intraband cutoff frequency can be determined either by the frequency where  $\sigma_1$  has a minimum or by the frequency where  $\sigma_2 < 0$ . As seen in Fig. 3 (c), since the YbAl<sub>3</sub> sample at room temperature did not have a  $\sigma_2$  zero-crossing, we used the former method which gave  $\omega_c \approx 1100$  cm<sup>-1</sup>. Since the high frequency Drude-Lorentz oscillator was centered around 2800 cm<sup>-1</sup>, this gave well defined separation between the intraband and interband oscillators. Hence, the intraband plasma frequency was given by the sum in quadrature of the plasma frequency of the two Drude oscillators, giving  $\omega_p = 2\pi \times (95 \pm 10)$  THz.

For LuAl<sub>3</sub>, the optical conductivity was parameterized by two Drude terms within our spectral range, both of which contributed to the total intraband plasma frequency. A plot of the temperature dependent spectral weight  $\omega_p^2$  for both YbAl<sub>3</sub> and LuAl<sub>3</sub> is shown in Fig. 4. The LuAl<sub>3</sub> film demonstrated a small decrease in the spectral weight with temperature. In YbAl<sub>3</sub> a small decrease was also observed as the temperature decreased below 50K. The decrease in the spectral weight given as  $\omega_p^2 = \frac{ne^2}{m}$  can be explained as a change in the carrier density *n*. This may be consistent with ARPES studies on these films which found that a large shift in the chemical potential as the temperature was decreased and

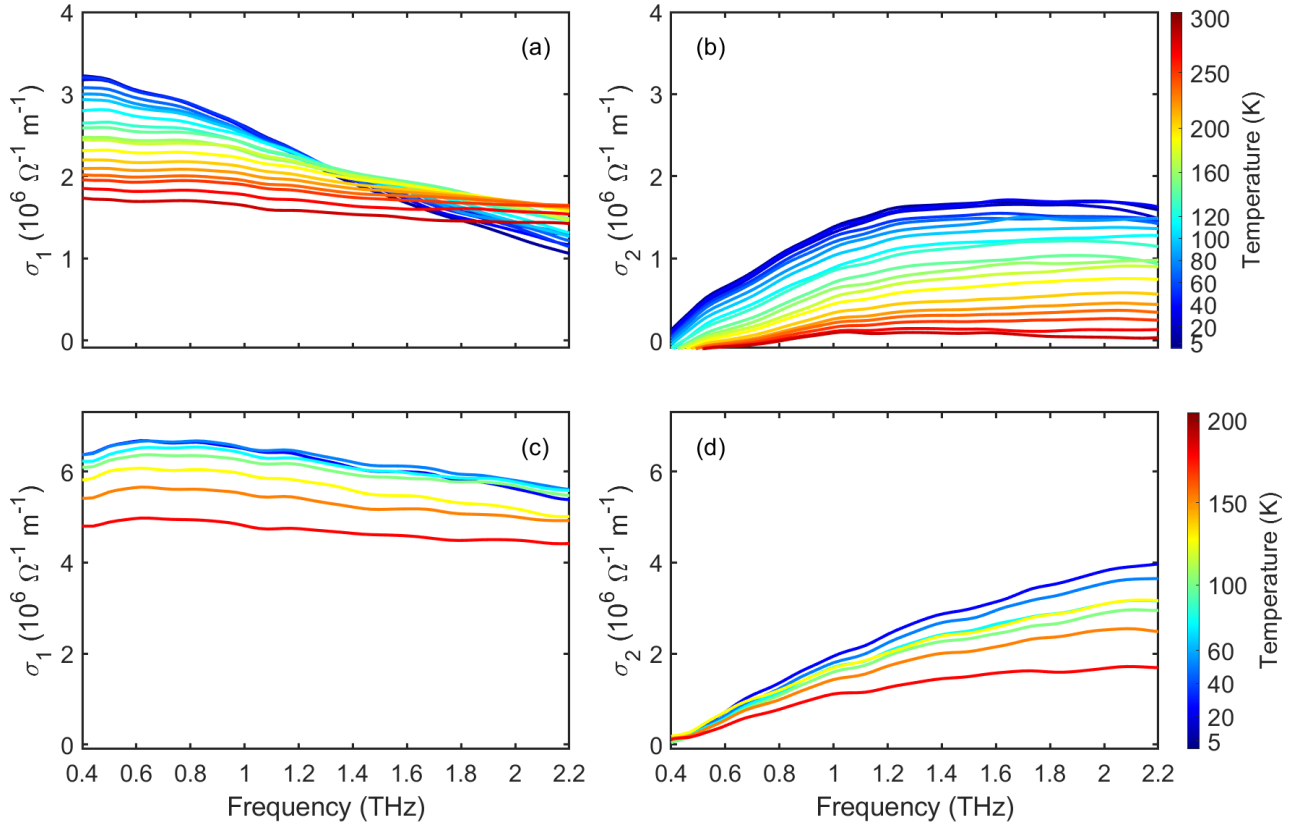


FIG. 2. (a), (b) Real and imaginary THz conductivity of  $\text{YbAl}_3$  as a function of frequency, (c), (d) Real and imaginary THz conductivity of  $\text{LuAl}_3$  as a function of frequency.

a Lifshitz transition occurred that elevated an electron pocket above  $E_F$  [16].

In Fig. 5 we present the extended Drude scattering rate as both a function of frequency and temperature. The frequency dependence of the scattering rate does not demonstrate major variation within our reduced spectral range. Examining the temperature dependence of the scattering rate taken along different frequency cuts, it is clear that the scattering rate becomes enhanced as the temperature is raised above 50 K and begins to show signs of saturation up to 300 K. Due to the phase space constraints on the quasiparticles scattering in the Fermi liquid regime, the scattering rate is expected to demonstrate  $\omega^2$  and  $T^2$  dependence. Nevertheless, on energy scales exceeding the correlation scale  $k_b T^* \approx 3.4$  meV, the quasiparticle description can begin to breakdown. Accordingly, we expect that any frequency dependence in the scattering rate would be more apparent at  $\omega < 0.8$  THz.

In Fig. 7 the extended Drude effective mass is presented. Below 1 THz, the effective mass seems to dip suddenly; for higher frequencies no significant frequency-

dependence is demonstrated. The suddenly may be an artifact of the conductance correction to account for the buffer layer. However, taking a frequency cut at 1 THz exhibits a gradual mass enhancement as the temperature is lowered. The magnitude of the effective mass renormalization is observed to be less than found from other experimental methods [13, 14]. The reason for the smaller mass enhancement seen is unclear, but could be related to disorder scattering in these relatively low residual resistivity ratio (RRR) films. As mentioned above, the residual resistivity ratios of these  $\text{YbAl}_3$  films are still much less than the approximately 60 found in high-quality single crystals [14]. It is reasonable to expect that strong scattering interferes with the formation of the mass enhanced state.

From the extended Drude analysis, it is clear that the behavior of the scattering rate and effective mass indicate that the crossover into the FL regime is not particularly sharp. Unlike other heavy-fermion compounds which can show a dramatic increase in the effective mass [8, 22], the weaker mass enhancement of quasiparticles and the slow crossover as a function of temperature has been pro-

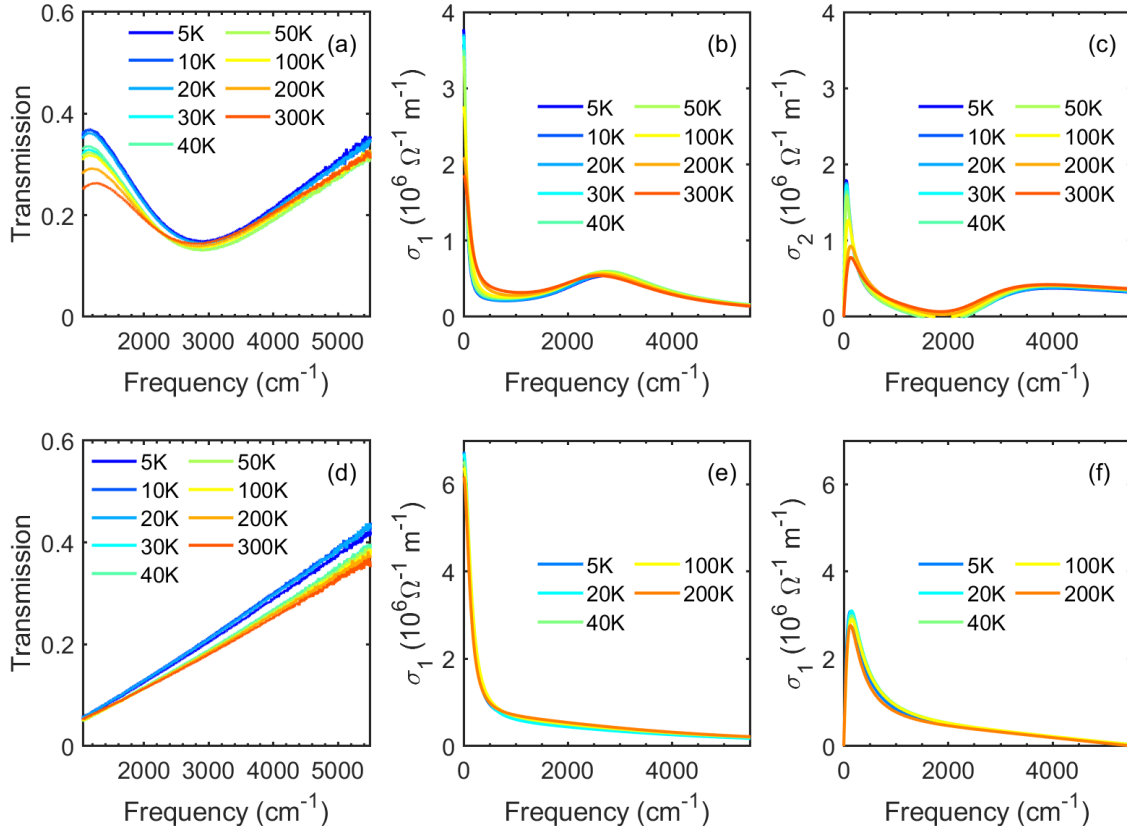


FIG. 3. MIR transmission shown above for  $\text{YbAl}_3$  (a) and  $\text{LuAl}_3$  (d). The real and imaginary parts of the optical conductivity modeled by the combined THz complex conductivity and MIR transmission is shown below in (b),(c) for  $\text{YbAl}_3$ . The real and imaginary parts of the optical conductivity for  $\text{LuAl}_3$  are shown in (e) and (f).

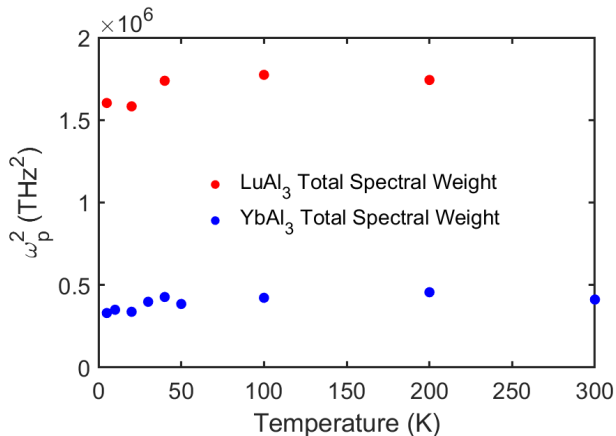


FIG. 4. The intraband spectral weight as a function of temperature deduced from simultaneous fitting of the THz and MIR data for  $\text{LuAl}_3$  and  $\text{YbAl}_3$ . While  $\text{LuAl}_3$  exhibits a small decrease in spectral weight, below 40 K the spectral weight of  $\text{YbAl}_3$  exhibits proportionally a larger decrease.

posed to originate from the mixed-valence states of Yb [11]. The two important energy scales in this material are set by the FL coherence temperature  $T^* = 40$  K and the Kondo temperature  $T_K = 670$  K. The evidence for a slow crossover in  $\text{YbAl}_3$  and related  $\text{YbXCu}_4$  compounds ( $X = \text{Ag, Cd, In, ...}$ ) [23] originates from residual low energy spectral weight even into intermediate temperatures [24]. In the extended Drude model, the effective mass is understood as the ratio of the spectral weight of the narrow Drude component over the spectral weight of the normal state,  $m^*(\omega)/m_b = \omega_p^*(\omega)^2/\omega_{p,normal}^2$ . This residual spectral weight will appear experimentally as an enhanced effective mass above the FL coherence temperature  $T^*$  and suggests that in  $\text{YbAl}_3$  hybridization effects are still present above  $T > 40$  K.

## CONCLUSION

The field of heavy-fermion physics is relevant to answering questions regarding exotic phenomena that

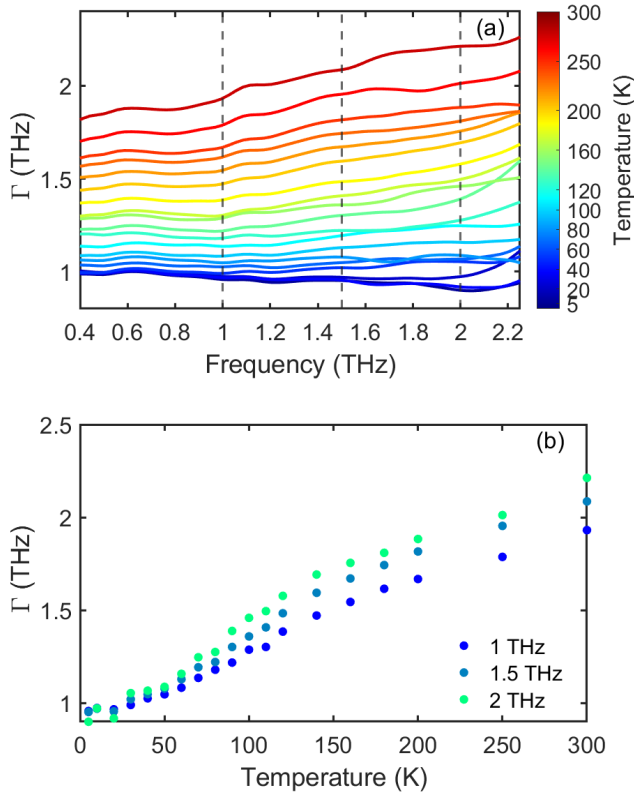


FIG. 5. Extended Drude scattering rate as a function of frequency (a) and temperature (b) taken along frequency cuts indicated by vertical dashed lines in the upper figure.

emerge from correlated electronic systems. The recent development of high-quality MBE thin films have allowed the first TDTS experiments to be conducted on  $\text{YbAl}_3$  and  $\text{LuAl}_3$ . The low energy scales of the heavy quasiparticles makes TDTS an ideal probe to study quasiparticle dynamics and enhance our understanding of these complex systems. This gives the opportunity for well-characterized systems to be studied carefully at the lowest energy scales.

From our results, we found that the  $\text{LuAl}_3$  film was well described by conventional Drude transport. The extended Drude formalism was used to study  $\text{YbAl}_3$  and the quasiparticle scattering rate demonstrates a similar  $T^2$  scaling up to the FL coherence temperature  $T^*$  consistent with 4-probe measurements. There was a moderate mass enhancement observed at the lowest temperatures. While some mass enhancement was observed, it was less than the scale suggested by dHvA measurements or specific heat. Nevertheless, there is still clear evidence for a well-established low-temperature FL state. The reason for the smaller mass enhancement is unclear, but it could be related to disorder scattering in these relatively low RRR films. From the extended Drude scattering rate,

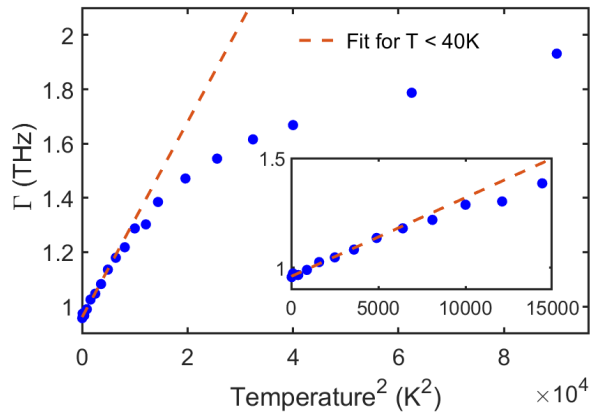


FIG. 6. Extended Drude scattering rate at 1 THz plotted against  $T^2$  to compare to FL predictions. Note the small discrepancy of the  $\Gamma \propto T^2$  fit above 40K at intermediate temperatures, suggestive of a slow crossover above  $T^*$ .

there is evidence for a slow crossover in the mass renormalization as found in other Yb-based mixed valence and heavy fermion compounds. At the lowest temperatures,  $1/\tau \propto T^2$  is followed up to 40 K, but the trend is still followed up to 100 K. Future experiments could be done in the microwave region down to lower temperatures to discern if quasiparticle behaviors demonstrate consistency with Fermi liquid predictions across a greater spectral range. Studying thicker films will also decrease the impact of the artifacts introduced using a multilayer conductance model.

- 
- [1] G. Stewart, Rev. Mod. Phys. **56**, 755 (1984), ISSN 02529262.
  - [2] P. Coleman, Phys. Rev. Lett. **59**, 1026 (1987), ISSN 00319007.
  - [3] Z. Fisk and M. B. Maple, J. Alloys Compd. **183**, 303 (1992), ISSN 09258388.
  - [4] B. Brandow, Phys. Rev. B **33**, 95 (1986).
  - [5] L. Degiorgi, Rev. Mod. Phys. **71**, 687 (1999), ISSN 00346861.
  - [6] A. Georges, G. Kotliar, W. Krauth, and M. J. Rozenberg, Rev. Mod. Phys. **68**, 13 (1996), ISSN 08958696.
  - [7] E. D. Bauer, C. H. Booth, J. M. Lawrence, M. F. Hundley, T. Ebihara, J. D. Thompson, and P. S. Riseborough, Phys. Rev. B **69**, 1 (2004), ISSN 1550235X.
  - [8] A. M. Awasthi, L. Degiorgi, G. Grüner, Y. Dalichaouch, and M. B. Maple, Phys. Rev. B **48**, 10692 (1993), ISSN 01631829.
  - [9] B. C. Webb, A. J. Sievers, and T. Mihalisin, Phys. Rev. Lett. **57**, 1951 (1986), ISSN 00319007.
  - [10] S. Nakatsuji, K. Kuga, Y. Machida, T. Tayama, T. Sakakibara, Y. Karaki, H. Ishimoto, S. Yonezawa, Y. Maeno, E. Pearson, et al., Nat. Phys. **4**, 603 (2008), ISSN 17452481.
  - [11] A. L. Cornelius, J. M. Lawrence, T. Ebihara, P. S. Rise-

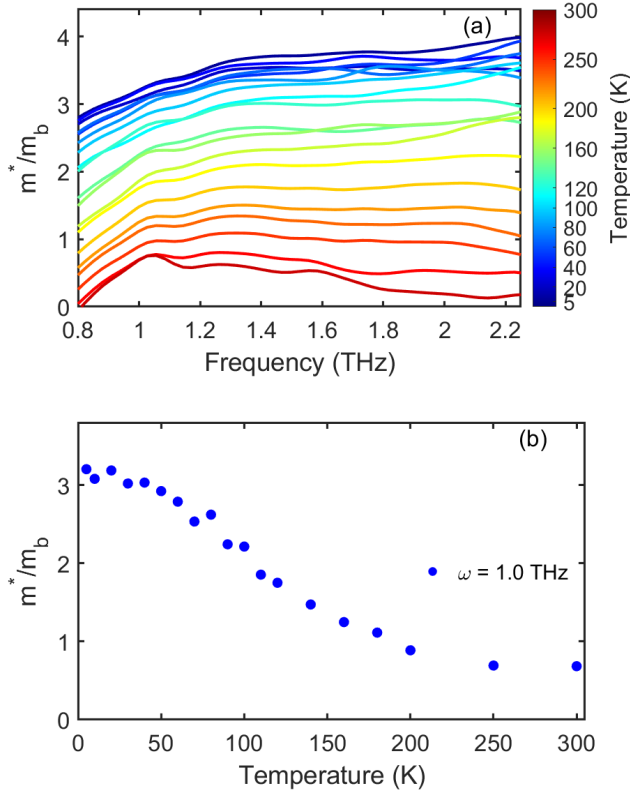


FIG. 7. Extended Drude effective mass as a function of frequency (a) and temperature (b) taken as a frequency cut at  $\omega = 1.0$  THz. The effective mass demonstrates a sharp decline below 1 THz which arises from a phase-sensitive artifact.

- borough, C. H. Booth, M. F. Hundley, P. G. Pagliuso, J. L. Sarrao, J. D. Thompson, M. H. Jung, et al., *Phys. Rev. Lett.* **88**, 4 (2002), ISSN 10797114.
- [12] L. Degiorgi, F. B. Anders, and G. Grüner, *Eur. Phys. J. B* **19**, 167 (2001), ISSN 14346028.
- [13] H. Okamura, T. Michizawa, T. Nanba, and T. Ebihara, *J. Phys. Soc. Japan* **73**, 2045 (2004), ISSN 00319015.
- [14] T. Ebihara, Y. Inada, M. Murakawa, S. Uji, C. Terakura, T. Terashima, E. Yamamoto, Y. Haga, Y. Onuki, and H. Harima, *J. Phys. Soc. Japan* **69**, 895 (2000), ISSN 00319015.
- [15] T. Ebihara, E. D. Bauer, A. L. Cornelius, J. M. Lawrence, N. Harrison, J. D. Thompson, J. L. Sarrao, M. F. Hundley, and S. Uji, *Phys. Rev. Lett.* **90**, 4 (2003), ISSN 10797114.
- [16] S. Chatterjee, J. P. Ruf, H. I. Wei, K. D. Finkelstein, D. G. Schlom, and K. M. Shen, *Nat. Commun.* **8**, 1 (2017), ISSN 20411723, 1710.07651.
- [17] S. Chatterjee, S. H. Sung, D. J. Baek, L. F. Kourkoutis, D. G. Schlom, and K. M. Shen, *J. Appl. Phys.* **120**, 1 (2016), ISSN 10897550, 1608.01045, URL <http://dx.doi.org/10.1063/1.4958336>.
- [18] A. B. Kuzmenko, *Rev. Sci. Instrum.* **76**, 1 (2005), ISSN 00346748, 0503565.
- [19] F. Marabelli and P. Wachter, *Phys. Scr.* **120** (1992).
- [20] P. Coleman, *Phys. Rev. B* **35**, 5072 (1987).
- [21] J. W. Allen and J. C. Mikkelsen, *Phys. Rev. B* **15**, 2952 (1977), ISSN 01631829.
- [22] G. Bossé, L. Pan, Y. S. Li, L. H. Greene, J. Eckstein, and N. P. Armitage, *Phys. Rev. B* **93**, 1 (2016), ISSN 24699969, 1405.4007.
- [23] J. M. Lawrence, P. S. Riseborough, C. H. Booth, J. L. Sarrao, J. D. Thompson, and R. Osborn, *Phys. Rev. B* **63**, 1 (2001), ISSN 1550235X.
- [24] H. Anzai, K. Morikawa, H. Shiono, H. Sato, S.-i. Ideta, K. Tanaka, T. Zhuang, K. T. Matsumoto, and K. Hirao, *Phys. Rev. B* **101**, 1 (2020), ISSN 2469-9950.